Design Methodologies for Robust Nano-Positioning

Abu Sebastian, *Member, IEEE,* and Srinivasa M. Salapaka, *Member, IEEE*

***Abstract*—In this paper, we present a systematic control design and analysis for a two-dimensional nano-positioner. The primary emphasis of the paper is on the robustness of the closed-loop device as these flexure-stage-based, piezoactuated nano-positioners are nonlinear and operate in diverse conditions. To this end, we have used many tools from modern control theory to model devices and to quantify device resolution, bandwidth, and robustness. The implementation of this procedure for the simultaneous achievement of the objectives of robustness, high precision and high bandwidth is presented. The merits of the paradigm are demonstrated through experimental results.**

***Index Terms*—Atomic force microscopy, flexure stages, Glover–McFarlane design, nano-positioning, piezoactuation, robust control.**

I. Introduction

THE past two decades have seen the rise and immense growth of nanoscience and nanotechnology. The invention of scanning probe microscopes such as the scanning tunneling (STM) and atomic force microscope (AFM) has revolutionized research in various areas such as biology, materials science, optics, precision mechanics, and micro-electronics [1]–[3]. The growth of research in these areas and the rapid rise in their applications [4]–[10] have in turn imposed new demands on nano-positioning where the need for higher precision at increasing bandwidth is presenting new challenges. The variety of these applications with operations in diverse condition necessitate *robust* control designs to meet these challenges.

There is a considerable literature that addresses performance issues and the compensation of the nonlinear effects of piezoactuation. Typically, the nano-positioning devices are actuated by piezoelectric materials. The advantages of these actuators are several: they provide repeatable subnanometer motion, do not have backlash, do not suffer from wear and tear, require very little maintenance, have fast response times, can generate large forces, are operable in a wide temperature range, and are not affected by magnetic fields. However, their use is hampered by nonlinear effects such as hysteresis, which can be as large as 10%-15% in large traversals, and creep, which become prominent in slow experiments [11], [12]. Many efforts have been made to counter the nonlinear effects including design changes in the open-loop implementation such as using 'harder' piezoceramics that have smaller nonlinear effects at the cost of travel range [13], replacing voltage control by charge control [14] which achieves lower hysteresis but leads to more creep, less travel and a lower positioning bandwidth; post-processing data obtained from actuations designed for prespecified trajectories [15], which are not useful for applications that require real time compensation, and compensating for the adverse nonlinear effects by a careful modeling of the nonlinearities, which achieves good results but is sensitive to the precision of the model used [16]. Compared with the open-loop architecture, there are fewer feedback design schemes for nano-positioning. In [17], the design of a feedback controller using an optical sensor attachment to enhance the performance of an AFM scanner is described. Similar efforts to improve the imaging speeds are made in [18]. Ref. [11] describes the $\mathcal{H}_\infty$ controller design for a one-dimensional nano-positioning system where high closed-loop bandwidths are achieved. In [12], a Smith predictor-based robust $\mathcal{H}_\infty$ controller is developed for a piezoactuator with an emphasis on countering hysteresis.

In this article, a large-range nano-positioner capable of positioning in two dimensions is presented. Flexure stages serve as sample positioners and are actuated by piezoelectric actuators. A preliminary version of this paper has appeared in [19]. The primary emphasis on the control design in this paper is to achieve robustness of the closed-loop device. In these large-range scanners, the robustness requirement is motivated by many reasons: the repeated use of flexure stages leads to time-varying changes in their stiffness, thus, uncertain pole locations; the unmodeled nonlinear effects are significant, and these devices are used in diverse operating conditions. Here we present two *robust* control designs motivated by different requirements. First, we present the Glover–McFarlane $\mathcal{H}_\infty$ design with the goal of increasing robustness of *existing industrial* control designs without significantly compromising device performance. Many of the existing controllers are designed to achieve specific tracking requirements (such as zero steady-state tracking) commonly needed in imaging applications. The Glover–McFarlane loop-shaping scheme provides a framework to robustify any existing design with a quantifiable compromise on the performance. In this methodology, it is possible to separate the designing task of meeting performance specifications (such as tracking requirements, bandwidth and resolution) and robustness into two modular steps. We demonstrate the robustness introduced by this design with a little compromise (sometimes even as improvement of) on performance by comparing results with that of the existing designs. Second, we present a robust $\mathcal{H}_\infty$ design to *simultaneously* achieve performance and robustness in these devices for applications where neither specific tracking requirement nor a characterization of uncertainty are available *a priori*.

Manuscript received February 20, 2004. Manuscript received in final form April 19, 2005. Recommended by Associate Editor S. Devasia. The work of A. Sebastian was supported in part by the National Science Foundation under Grant CMS-0201560 and in part by a DARPA-UCLA sub-contract to Iowa State University under the MOSAIC initiative to Prof. Murti V. Salapaka.

A. Sebastian is with the IBM Zürich Research Laboratory, CH-8803 Rüschlikon, Switzerland (e-mail: ase@zurich.ibm.com).

S. M. Salapaka is with the Department of Mechanical and Industrial Engineering, University of Illinois, Urbana, IL 61801 USA (e-mail: salapaka@uiuc.edu).

Digital Object Identifier 10.1109/TCST.2005.854336

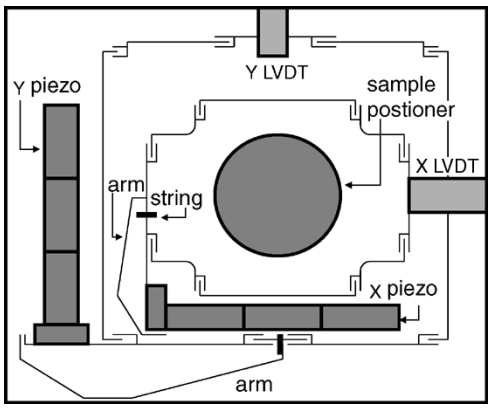

Fig. 1. Schematic of the nano-positioning device. There are two stages "X" and "Y," with "X" located on top of "Y." Each stage is actuated by piezoelectric stacks and the resulting motion is sensed by LVDT sensors.

The paper is organized in the following way. In Section II, a description of the device is given. This is followed by a frequency-domain-based system identification described in Section III. The control design and the experimental results are presented in Section IV. The device characterization is presented in Section V.

II. Device Description

The nano-positioning system studied in this article is described in Fig. 1 (developed in Asylum Research, Santa Barbara, CA).

The flexure stage consists of two stages, with "X" located on "Y" (Fig. 1), with the sample holder on the "X" stage. Each stage, by virtue of the serpentine spring design, deforms under the application of force, providing motion. These forces are generated by stack-piezos. As shown in Fig. 1, there are three piezoactuators in series for each axis. The motion of each stage is measured by the corresponding linear variable differential transformer (LVDT) and the associated demodulation circuit.

Besides being cheaper, the piezostacks have longer travel ranges than their cylindrical counterparts used more often in industry. These actuators lead to a travel range of approximately 100 μm in both directions. The modified LVDT sensors used have resolution in the order of 2 Å over 1-kHz bandwidth, which gives a vast advantage over more common optical sensors. The control laws are implemented on an Analog Devices ADSP-21160 digital signal processor.

III. Identification

The complex structural design makes physical modeling of the device difficult. The model has been inferred using frequency-response-based techniques. The device is viewed as a two-input two-output system in which the low-voltage signals to the "X" and "Y" amplifiers (u_x and u_y) are the inputs and the motion of "X" and "Y" stages (x and y) measured by the corresponding LVDT sensors, are the outputs. This results in four input–output transfer functions G_{ij}, $i, j \in \{x, y\}$. Here G_{ij} represents the transfer function from input j to output i. Fig. 2 depicts the different blocks constituting the mapping between u_x and x.

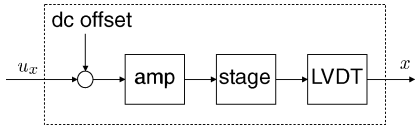

Fig. 2. Blocks constituting the mapping between u_x and x.

These maps can be assumed to be linear over a small region of operation about an operating point. A dc offset is applied to maintain a particular operating point (Fig. 2). The nominal operating point is chosen to be the *null position*, i.e., where the LVDT outputs read zero. Frequency responses are obtained about this operating point to obtain the nominal model (that maps $(u_x\ u_y)'$ into $(x\ y)'$) denoted by

$$G = \begin{bmatrix} G_{xx} & G_{xy} \\ G_{yx} & G_{yy} \end{bmatrix}.$$

The responses are obtained using an HP3536A signal analyzer with 10 mV amplitude forcing and are averaged over 200 measurements for a bandwidth of 1.25 kHz. Note that the forcing signal is small as the total input range is 10 V which corresponds to approximately 100 μm travel range. Rational transfer functions are fit to responses. $G_{xx}(s)$ is a seventh-order transfer function with the first resonance frequency at approximately 390 Hz. $G_{yy}(s)$ is fifth-order, with the first resonance frequency at 235 Hz. $G_{xx}(s)$, $G_{yx}(s)$, and $G_{yy}(s)$ are given in the following:

$$G_{xx}(s) = \frac{4.29\times10^{10}(s^2+631.2s+9.4\times10^6)}{(s^2+178.2s+6\times10^6)(s^2+412.3s+1.6\times10^7)} \times \frac{(s^2+638.8s+4.5\times10^7)}{(s^2+209.7s+5.6\times10^7)(s+5818)}$$

$$G_{yx}(s) = \frac{-28.7(s-5094)}{s^2+94.7s+6.48\times10^6}$$

$$G_{yy}(s) = \frac{1.38\times10^{10}}{(s+6165)(s^2+101.7s+2.18\times10^6)} \times \frac{(s^2+1006s+1.625\times10^7)}{(s^2+708.1s+2.7\times10^7)}.$$

G_{xy} and G_{yx} were found to be relatively small compared with G_{xx} and G_{yy}. Fig. 3(A) and (B) shows how well the frequency responses obtained from these models agree with those obtained experimentally. Owing to the piezoactuation and the changing flexure dynamics, these models were found to vary with different operating points and with time. To study the variation with respect to the operating points, frequency responses are obtained at different operating points. A considerable variation was observed in these responses. Fig. 3(C) shows the responses obtained at different operating points spread over a range of approximately 80 μm, separated by approximately 20 μm. In addition, it was observed that the frequency response at the same operating point varies when obtained at different times. This time varying uncertainty typically manifests itself as a change in the resonance locations. This is again an artifact of the flexure stage. Repeated cycling at significant strains (such as in the case of the nanopositioner discussed here) could lead to changes in Young's modulus of the flexure through effects such as strain hardening [20]. This translates into changes in the spring constants and, hence, a change in the pole positions. The mass of the objects

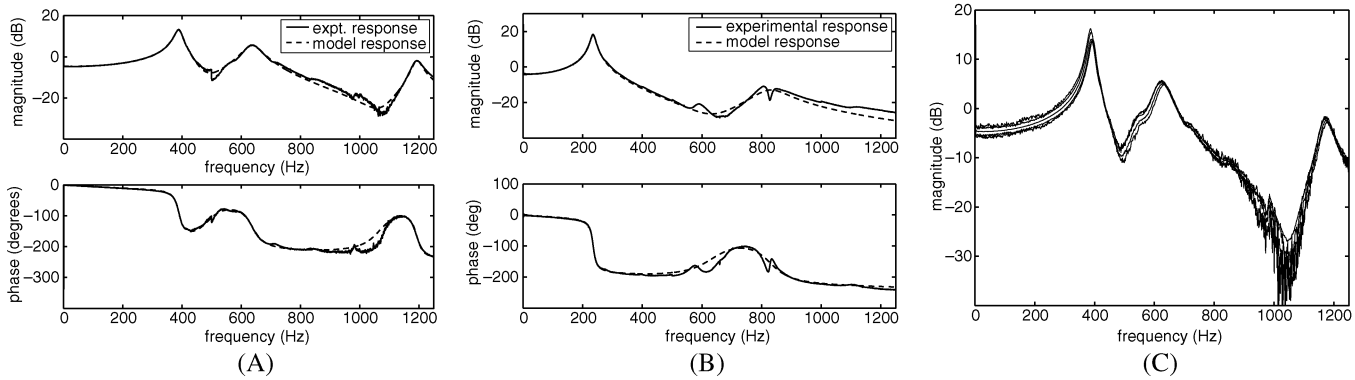

Fig. 3. (A), (B) Experimental frequency responses are compared with the responses of the nominal models $G_{xx}(s)$ and $G_{yy}(s)$. (C) Experimentally obtained frequency responses at different operating regions for the X stage.

which are being positioned could also affect the frequency response of the positioner. However, owing to the relatively large mass of the flexure stage, this effect is not very pronounced. All these uncertainties make robustness of the closed-loop system a key requirement.

IV. Controller Design and Implementation

In the design of the feedback laws, the coupling transfer functions G_{xy} and G_{yx} are neglected in order to simplify the design process. This is reasonable as the coupling terms are relatively small. The mode of operation of this device is such that higher bandwidth requirements are made on the smaller stage "X" whereas the "Y" stage is made to move relatively slow. Hence, there is a greater emphasis on the control designs for the "X" stage, which is presented in this paper. Designs were also done for G_{yy}, and the resulting diagonal controllers were implemented, the details of which are not presented in this paper. Fig. 4 shows the unity feedback loop for the "X" stage. In this figure, x_r is the reference signal, x is the output signal, and K_{xx} is the control transfer function that needs to be designed. The error e_x is given by $e_x = x_r - x = Sx_r - Tn_x$, where S is the sensitivity function and T the complementary sensitivity function. The closed-loop bandwidth of the nano-positioner is defined to be the frequency at which $|S(j\omega)|$ crosses -3 dB. As T is the transfer function between e and the noise n, it is a measure of the resolution. As mentioned earlier, the primary emphasis of this paper is on robustness. $\|T\|_\infty$ and $\|S\|_\infty$ are good measures of the robustness of the device (for appropriate uncertainty classes) and will be used frequently in subsequent discussions for comparing the robustness of various design schemes. In particular, these values give a lower bound on the gain and phase margins. These lower bounds given in terms of $\|S\|_\infty$ are GM $= \|S\|_\infty/(\|S\|_\infty - 1)$ and PM $= 2\sin^{-1}(1/2\|S\|_\infty)$ [21].

A. Control Designs

For robust nano-positioning, two approaches are employed. In the first approach, Glover–McFarlane robustifying controllers are designed for existing controllers typically employed in nano-positioners. In the second approach, robust $\mathcal{H}_\infty$ designs are employed to meet the bandwidth and tracking requirements along with the required robustness.

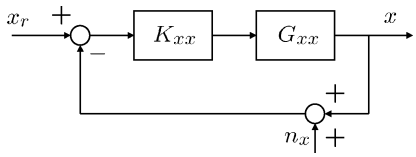

Fig. 4. Unity feedback configuration for G_{xx}.

1) Robustification of Existing Controllers:

a) Proportional double integral control design: Proportional integral (PI) and proportional double integral (PII) controllers are the most common forms of controllers currently used for nano-positioning in the scanning-probe industry. Their popularity stems from the fact that they are simple to implement. Moreover an attractive feature of these controllers is that they can track ramp signals (common in imaging applications) with zero steady-state error. The PII controller has the structure $k_p + k_i/s + k_{ii}/s^2$. Here a PII design is presented that has been obtained after considerable search and tuning over the parameter space. It is given by $K_{\text{pii}}(s) = (0.001s^2 + 450s + 10^5)/s^2$. A plot of $S(j\omega)$ is shown in Fig. 5(A). Besides having a low closed-loop bandwidth of 31 Hz, this design has poor robustness properties. The $\|S\|_\infty$ for K_{pii} is 15.5 dB, which is unsatisfactory and leads to sustained oscillations and instability while performing large-range scans.

The PII controller was implemented, and Fig. 5(B) shows the tracking of 1 Hz and 5 Hz triangular waves. The tracking errors at turn around points are large as these contain higher harmonics that the device does not track. However, this is not a significant problem as the data corresponding to this region is discarded in typical imaging applications. But it is important that in the midregions, the triangular wave is tracked satisfactorily. The 5-Hz tracking is unsatisfactory as the error is substantial over the entire trajectory. Fig. 5(B) shows that the usable region of the trajectory is only 30% of the total period. The oscillatory behavior is due to the peaks present in $|S(j\omega)|$ [see Fig. 5(A)]. Owing to the low phase margin, attempts to introduce a low-pass filter within the loop to improve the resolution results in instability. Moreover it is commonly observed that the PII controller becomes unstable or starts exhibiting oscillatory behavior while scanning over large scan ranges.

b) Glover–McFarlane control design: The PII designs are nonrobust and fail to achieve large closed-loop bandwidths.

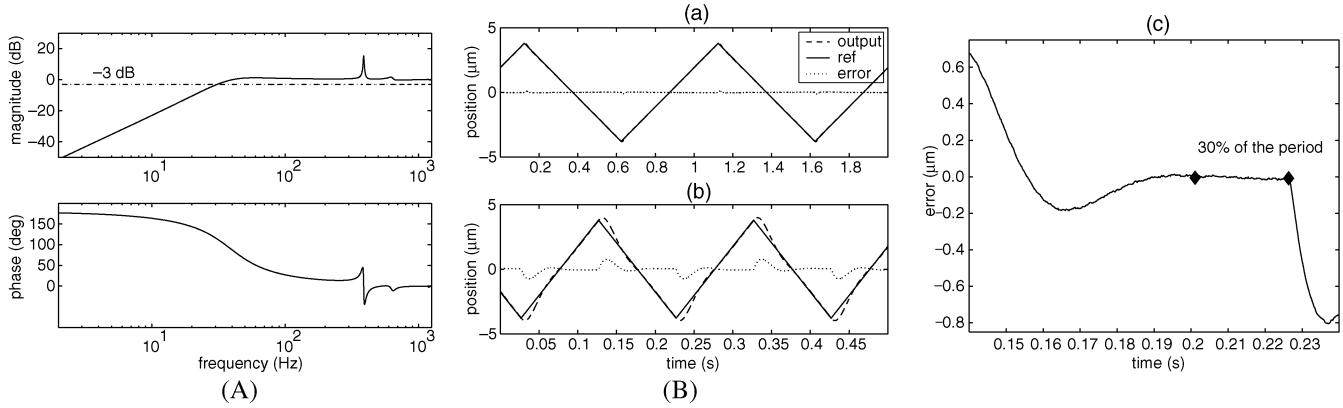

Fig. 5. (A) Bode plot of the sensitivity function is shown for a PII controller. The peaks in the magnitude plot indicate lack of robustness. (B) Shows the tracking of triangular reference signals using $K_{\rm pii}$. (a) Tracking of a 1-Hz triangular signal is shown. (b) At 5 Hz, oscillatory behavior is observed. (c) This reduces the region of the trajectory which can be used for scanning purposes.

Moreover, the designs are tedious as they require tuning over multiple parameters. These parameters are designed to shape the open-loop transfer function $T_{ol} = \text{GK}$ so that it has high gains at low frequencies and low gains at high frequencies. The resulting high gains at low frequencies imply better tracking of reference signals, and the low gains at high frequencies provide better device resolution by ensuring noise attenuation in the feedback signals. Moreover, the PII controllers ensure that the device tracks ramp signals with zero steady-state error. However, these designs do not account for uncertainties in the plant model and therefore do not guarantee robustness. These control laws are sensitive to these model uncertainties (as seen from the large values of $||S||_\infty$), and therefore the closed-loop performance in actual experiments deviates considerably from that predicted by the design.

The elegant control design introduced by Glover and McFarlane [22], [23] addresses both the performance and the robustness requirement. In this design, the model uncertainties are included as perturbations to the nominal model, and robustness is guaranteed by ensuring that the stability specifications are satisfied for the *worst-case* uncertainty. A remarkable feature of this design is that it achieves robustness with marginal reduction in performance. In fact, it is able to quantify the reduction by determining explicit bounds on how much it changes the loop gains at low and high frequencies. This design process consists of two steps.

Step 1) Design for performance: In this step, a shaping transfer function K_s is designed to meet the performance requirements such as high loop gain in low frequencies and low loop gain in high frequencies. At this stage the requirements for robustness and even stability are not considered. In the design presented in this paper, K_s is set equal to PII/PIID controllers. This is done to retain the closed-loop property of tracking ramp signals with zero steady-state error. Another reason is the prevalent use of such controllers in nano-positioning to realize performance specifications.

Step 2) Design of a robustifying controller: In this step, a robustifying controller K_r is obtained that provides good robustness properties to the closed-loop system obtained from the shaped plant $G_s = K_s G_{xx}$ of the previous step.

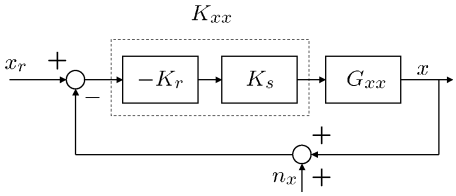

Fig. 6. Shaping controller is denoted by K_s and the robustifying controller by K_r.

More specifically, let $G_s = N/M$ be the normalized coprime factorization of the nominal shaped plant. The normalized coprime factor uncertainty characterization is given by

$$\left\{ \frac{N+\Delta_N}{M+\Delta_M} : \|[\Delta_N \quad \Delta_M]\| \leq \epsilon \right\}.$$

The robustifying controller should stabilize all the plants belonging to the previous set for a specified ϵ. For a shaping controller K_s, the maximum possible ϵ, $\epsilon_{\max}$ can be calculated *a priori* as shown in the following. The robustness margin ϵ is chosen to be slightly less than $\epsilon_{\max}$.

The following steps yield the optimal controller that assume a state–space model (A, B, C, D) available for the transfer function $G_s = K_s G_{xx}$.

Step 1) Let $\gamma = 1/\epsilon$. Obtain Z by solving the algebraic Riccati equation (ARE)

$$(A - BS^{-1}D^T C)Z + Z(A - BS^{-1}D^T C)^T - ZC^T R^{-1} CZ + BS^{-1}B^T = 0$$

where $R = I + DD^T$ and $S = I + D^T D$.

Step 2) Obtain X by solving the ARE

$$(A - BS^{-1}D^T C)^T X + X(A - BS^{-1}D^T C) - XBS^{-1}B^T X + C^T R^{-1} C = 0.$$

Step 3) The state–space realization of the robustifying controller K_r is given by

$$\left[\begin{array}{c|c} A+BF+\gamma^2 (L^T)^{-1} ZC^T (C+DF) & \gamma^2 (L^T)^{-1} ZC^T \\ \hline B^T X & -D^T \end{array}\right]$$

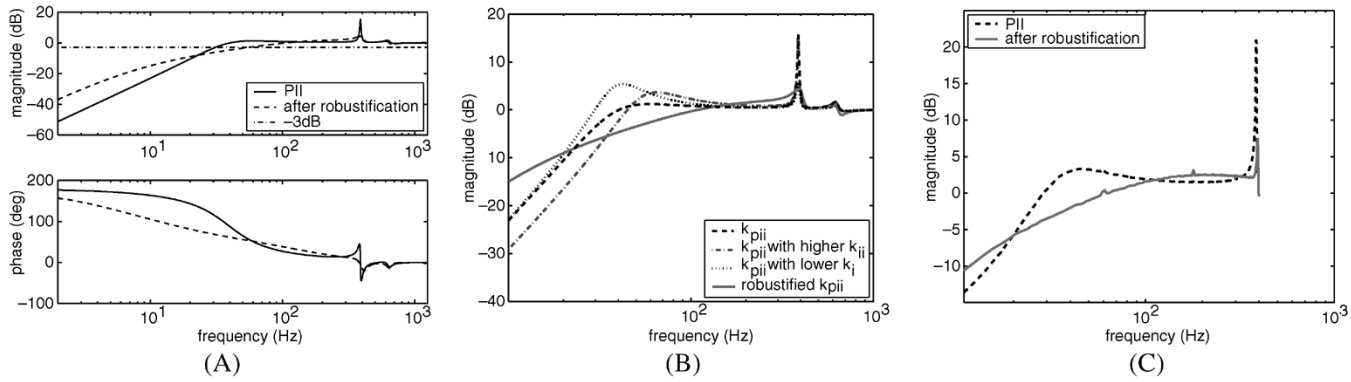

Fig. 7. (A) This plot illustrates the reduction in $\|S\|_\infty$ value due to Glover–McFarlane robustification. (B) The control design can be viewed as the shaping of the sensitivity function while satisfying the Bode integral formula. An increase in the gain of the PII controller results in two significant peaks appearing in the plot of $|S(j\omega)|$. Without any model information, it is not possible to reduce the two peaks by varying the PII coefficients without compromising on the bandwidth significantly. The robustifying controller with its model information shapes S in such a way that both the peaks are reduced in magnitude at the expense of marginal performance. (C) Experimentally obtained $S(j\omega)$ of $K_{\rm pii}$ before and after robustification.

where $F = -S^{-1}(D^TC + B^TX)$ and $L = (1 - \gamma^2)I + XZ$. The control loop to be implemented is shown in Fig. 6.

From a broad perspective, the optimization problem decomposes into two subproblems of "optimally" estimating the states of the shaped plant and of using these states to design an "optimal" control law. X captures the estimator component of the problem and Z the controller component. The maximum possible ϵ for the given shaped plant is given by $\epsilon_{\max} = (1 + \rho(XZ))^{-1/2}$, where ρ denotes the spectral radius. Hence, in this design scheme there is no need for an explicit characterization of uncertainty. The method detects and solves for the worst-case scenario.

As mentioned earlier, an important feature of the Glover–McFarlane design is that the loop transfer functions before and after robustification are not significantly different. In fact, in [23] it is shown that when $|G_s(j\omega)| > \sqrt{1/\epsilon^2 - 1}$

$$|K_r(j\omega)| \geq \frac{|G_s(j\omega)| - \sqrt{\frac{1}{\epsilon^2} - 1}}{\sqrt{\frac{1}{\epsilon^2} - 1}\,|G_s(j\omega)| + 1}$$

and when $|G_s(j\omega)| < 1/\sqrt{1/\epsilon^2 - 1}$

$$|K_r(j\omega)| \leq \frac{|G_s(j\omega)| + \sqrt{\frac{1}{\epsilon^2} - 1}}{1 - \sqrt{\frac{1}{\epsilon^2} - 1}\,|G_s(j\omega)|}.$$

The previous inequalities show that in the frequency regions where $|G_s(j\omega)|$ is big and in those where $|G_s(j\omega)|$ is small, there is a bound on the extent to which the robustifying controller changes the loop shape.

c) Robustification of $K_{\rm pii}$: The design process was applied to G_{xx} with K_s set to $K_{\rm pii}$ from Section IV-A1. A ninth-order robustifying controller K_r was obtained

$$\frac{5227.6(s+5818)(s+31.45)(s^2+160.3s+5.98\times10^6)}{(s+2797)(s+5684)(s+294.8)(s^2+386.2s+6.6\times10^6)} \times \frac{(s^2+209.6s+5.6\times10^7)}{(s^2+397.3s+1.66\times10^7)(s^2+203.3s+5.62\times10^7)}.$$

Fig. 7(A) compares the simulated sensitivity functions for a design with K_s before and after robustification. The much lower $\|S\|_\infty$ value indicates higher robustness. A careful examination of the sensitivity functions of PII controllers reveals the presence of two distinct peaks: a low-frequency peak and one near the resonance of the plant. The low-frequency peak arises from the Bode integral formula

$$\int_0^\infty \ln|S(j\omega)|\,d\omega = 0$$

to be satisfied by a loop transfer function, T_{ol} with relative degree two and no poles in the open RHP. Assume that for some $\alpha > 0$, $|S(j\omega)| \leq e^{-\alpha}$ in the frequency region $[0, \omega_1]$. The parameter α is a measure of the tracking performance. From the Bode integral formula, the following condition needs to be satisfied:

$$\int_{\omega_1}^\infty \ln|S(j\omega)|\,d\omega \geq \alpha\omega_1.$$

Moreover it can be shown that there exists $k > 0$ and ω_2 such that the loop transfer function satisfies, $|T_{ol}(j\omega)| \leq k/\omega^2$ for all $\omega \in [\omega_2, \infty]$. This added rolloff condition, which is essential for good resolution, makes the Bode integral effectively a "finite" integral that results in the appearance of the low-frequency peak in the S frequency response.

It can be seen that an increase in k_i primarily results in an increase in the magnitude of the high-frequency peak whereas an increase in k_{ii} results in an increase in the magnitude of the low-frequency peak as seen in Fig. 7(B). Both peaks are unsuitable for nano-positioning as they introduce low- and high-frequency oscillations while tracking. As Fig. 7(B) shows, varying k_i and k_{ii} does not reduce the peaks significantly without substantial compromise on bandwidth. But the robustifying controller with the added model information shapes the sensitivity function in such a way that the low- and high-frequency peaks are reduced in magnitude simultaneously with marginal compromise on bandwidth.

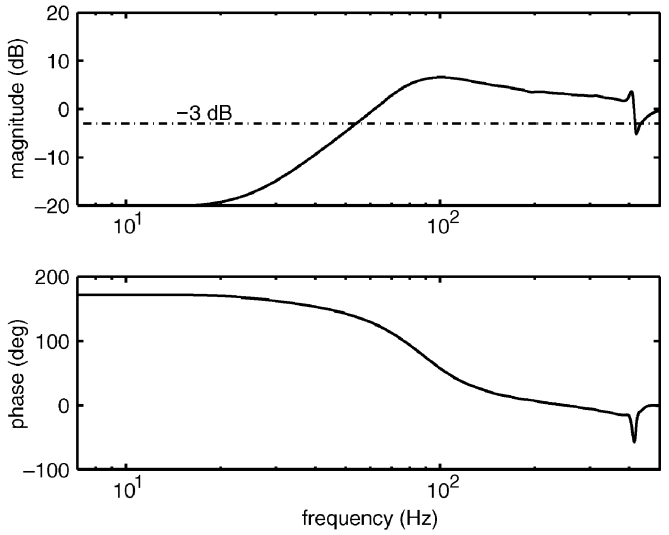

Fig. 8. Experimentally obtained sensitivity function of an aggressive (high bandwidth) Glover–McFarlane design.

Fig. 7(C) compares the experimentally obtained $|S(j\omega)|$ for K_{pii} before and after robustification. There is substantial reduction in the peak of $|S(j\omega)|$ owing to the robustifying controller. Note that the bandwidth is comparable for both, in spite of the significant difference in robustness.

d) Designs for higher bandwidth: In Step 1) of the proposed two-part design, the controller being designed for performance *does not have to result in a stable closed-loop map*. Thus, for example, considerably more aggressive PII controllers can be implemented with the help of robustification.

Fig. 8 depicts the experimentally obtained $S(j\omega)$ of a high-bandwidth Glover–McFarlane design. The design corresponds to a PII controller $(0.001s^2+600s+6\times10^5)/s^2$. The PII controller if used without robustification results in instability of the closed loop. However, with robustification, the design is stable and guarantees good robustness margins with the added benefit of increased performance. This plot shows a significant increase in bandwidth (>55 Hz) without much loss in robustness ($\|S\|_\infty = 1.7$).

Triangular signals are tracked using the implemented Glover–McFarlane designs. Fig. 9 illustrates the tracking of 5- and 10-Hz signals using the aggressive Glover–McFarlane design. Except for the turn-around points, the tracking error is small. For the 5-Hz triangular signals, approximately 70% of the period is usable in this case, compared with 30% for K_{pii} in spite of the larger amplitude of the reference waveform. Moreover these controllers are remarkably robust, allowing the use of filters inside the loop to improve resolution.

As the performance and robustness requirements are decoupled, Glover–McFarlane controllers can be used to robustify commonly used controllers such as PII that have features like zero steady-state error for ramp tracking. This is a significant advantage particularly when the nano-positioner is used for scanning applications. But in applications where robustification of existing controllers is not required, particularly in applications such as nanolithography where zero steady-state error ramp tracking is not essential, single-step designs like $\mathcal{H}_\infty$ can be employed, which is addressed next.

2) Robust $\mathcal{H}_\infty$ Control Design:

a) Nominal $\mathcal{H}_\infty$ control design: One of the disadvantages of classical control design processes is that an exhaustive search over the space of controller parameters is needed to meet bandwidth and resolution requirements. Also, in these designs, the open-loop transfer function is shaped even if these requirements are made on the closed-loop transfer function. In the nominal $\mathcal{H}_\infty$ design, the control law is obtained as a solution to an optimization problem that incorporates the performance objectives in its cost function. In this design, the performance requirements are imposed directly on the closed-loop transfer functions S, T and KS using appropriate weighting functions. As the error $e_x = Sx_r - Tn_x$, the bandwidth requirement is imposed on S. The requirement of high resolution is translated to a rolling-off of T at high frequencies. A bound on KS can be used to limit the control effort, u_x because $u_x = KSx_r$. In this design, a controller transfer function is obtained through an iterative process [21] such that $\left\| \begin{matrix} w_pS \\ w_TT \\ w_uKS \end{matrix} \right\|_\infty \leq 1$, where w_p, w_T and w_u are the weighting functions we design. Such a controller guarantees $\|w_pS\|_\infty \leq 1$, $\|w_TT\|_\infty \leq 1$ and $\|w_uKS\|_\infty \leq 1$. These weighting functions are designed to specify the frequency information of the performance objectives and system limitations. The transfer function, w_p, was chosen such that it has high gains at low frequencies and low gains at high frequencies. This scaling ensures that the optimal feedback law is such that the sensitivity function is small at low frequencies, thus, guaranteeing good tracking at the frequencies of interest. More precisely, w_p was chosen to be $(0.67s^2+769.5s+2.2\times10^5)/(s^2+9.425s+22.1)$ to achieve a closed-loop bandwidth of 75 Hz and to induce a 40-dB slope for S, which approximates a double integrator (to have better ramp tracking). The weighting function, $w_T = (s+571.2)/(0.01s+628.3)$ was chosen such that it has low gains at high frequencies and high gains at low frequencies. This was done to ensure the rolling-off of the complementary sensitivity function at high frequencies to have noise attenuation and thereby better resolution. Fig. 10(A) depicts $|w_p(j\omega)|$ and $|w_T(j\omega)|$.

The weighting function for the control w_u was chosen to be a constant given by $w_u = 1/10$. This ensured that the piezo signals were within saturation limits. A tenth-order controller was obtained from this design that has a bandwidth of 104 Hz. The controller was found to be nonrobust and to have poor noise characteristics after implementation. The reason for this behavior is that the nominal $\mathcal{H}_\infty$ design does not account for pole uncertainties, which are crucial for G_{xx} because of its lightly damped poles. The nominal $\mathcal{H}_\infty$ controller has zeros at 389 Hz, which is a dominant pole of G_{xx} which is also lightly damped. See [24] for a detailed description of these pole-zero cancellations in nominal $\mathcal{H}_\infty$ designs. Nominal $\mathcal{H}_\infty$ designs without consideration for robustness was found to be inappropriate for the nano-positioner. Robust $\mathcal{H}_\infty$ designs that account for pole uncertainties are one way of tackling this problem at the expense of bandwidth.

b) Robust $\mathcal{H}_\infty$ design: In this design, The pole uncertainty in G_{xx} is characterized using multiplicative uncertainty. The poles (those corresponding to the primary resonances) are varied

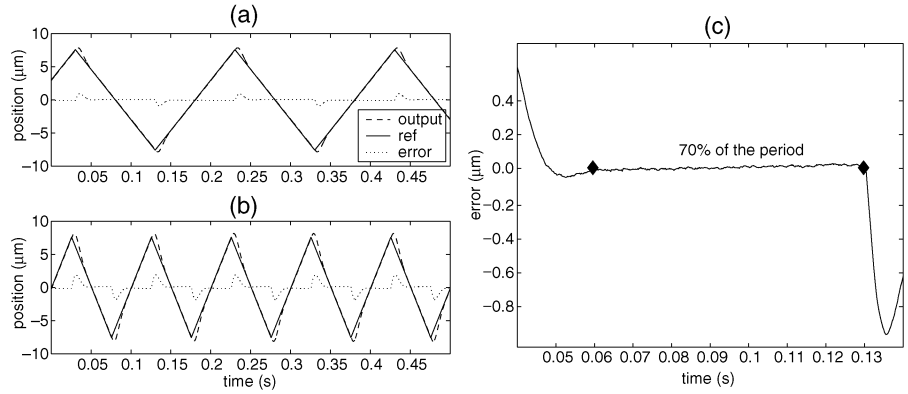

Fig. 9. (a) Tracking of 5-Hz triangular signals using a Glover–McFarlane controller. (b) Tracking of a 10-Hz signal using the Glover–McFarlane controller. Except for the turn around regions, the tracking is very good. (c) For the 5-Hz triangular signals, almost 70% of the period is usable in this case.

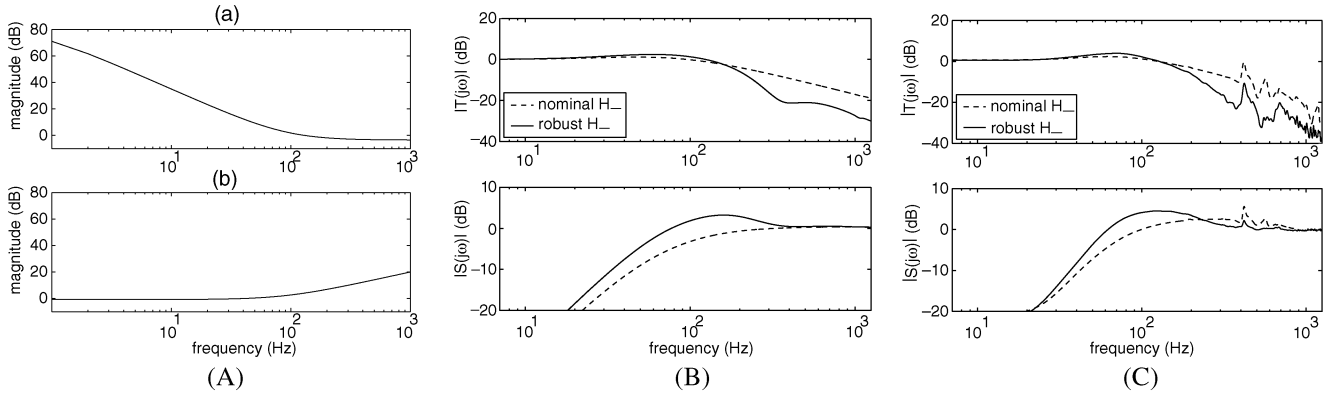

Fig. 10. (A) (a) Weighting function for the sensitivity function. The 40 dB roll off is to approximate a double integral action which enables steady-state ramp tracking. (b) The weighting function for the complimentary sensitivity function. (B) Analytical S and T frequency responses for nominal and robust $\mathcal{H}_\infty$ designs. (C) The experimentally obtained sensitivity and complementary sensitivity functions are compared for nominal and robust $\mathcal{H}_\infty$ designs.

over a certain regime, and their corresponding frequency responses are plotted. $w_i(s)$ is obtained such that these responses are captured by the perturbed plants $G_{xx}(s)(1+w_i(s)\Delta)$, where $\|\Delta\|_\infty < 1$. It can be shown that if a controller has to satisfy $\|w_pS\|_\infty \leq 1$ for plants belonging to a class $\mathcal{G}_{xx} = \{G_{xx}(1 + w_i\Delta) : \|\Delta\|_\infty \leq 1\}$, then it is sufficient that $\left\| \begin{matrix} w_pS \\ w_iT \end{matrix} \right\|_\infty \leq 1/\sqrt{2}$ is satisfied [21]. So in the original nominal $\mathcal{H}_\infty$ problem, the selection of $w_T = w_i$ fetches robust performance instead of just nominal performance. For G_{xx}, w_i was selected to be

$$w_i(s) = \frac{0.84s^2 + 2214s + 5.3 \times 10^6}{s^2 + 575.5s + 6.12 \times 10^6}.$$

In the original $\mathcal{H}_\infty$ problem, w_T was chosen to be w_i to incorporate the added robust performance requirement. The resulting controller was eleventh order. A comparison of the analytical closed-loop transfer functions of the two designs is shown in Fig. 10(B). The experimental plots are compared in Fig. 10(C). It can be seen that the experimental closed-loop transfer-function plots have some features that are absent in the analytical plots. This is due to uncertainty in the plant model, particularly pole uncertainty. Fig. 10(C) shows the experimental result of how the robust design introduces a dip in this frequency region, thus, reducing the magnitude of these unwanted peaks (Fig. 10(C) shows a fivefold reduction in the unwanted peak near the dominant pole location due to the robust design). Note that this comparison studies steady-state responses of the two designs and does not analyze the differences in the corresponding transient responses.

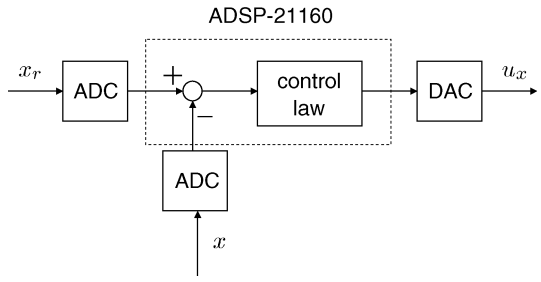

Fig. 11. Schematic of the controller hardware.

B. Implementation of the Controllers

The controllers designed in Section IV-A were discretized and implemented on an Analog Devices ADSP-21160 Digital Signal Processor. A schematic of the control system is shown in Fig. 11. The analog signals were sampled at 100 kHz. The discretized controllers were split into biquad sections (second-order sections), and each biquad was implemented in a Direct Form II IIR structure. This cascade implementation allows optimum pole-zero pairing and ordering, which can be used to counter finite-word-length effects [25]. Fig. 12 shows the direct

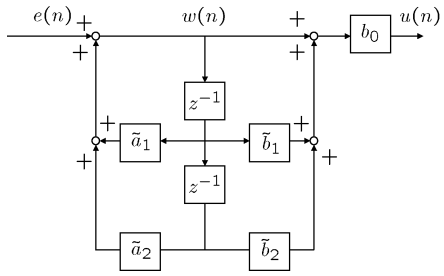

Fig. 12. Controllers were split into second-order sections (biquads) and each of them was implemented in a direct form II IIR structure depicted previously. The computational time for one biquad is 24 ns. $\tilde{b}_1 = b_1/b_0$, $\tilde{b}_2 = b_2/b_0$, $\tilde{a}_1 = -a_1$ and $\tilde{a}_2 = -a_2$.

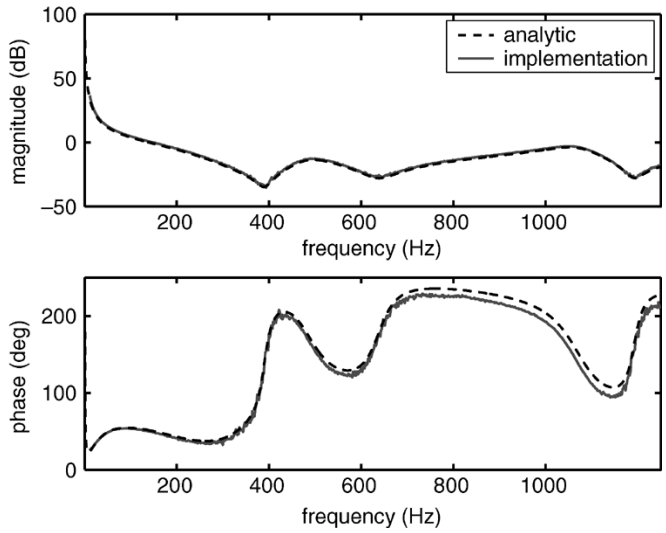

Fig. 13. Experimentally obtained frequency response of an implemented robust $\mathcal{H}_\infty$ controller is compared with the analytical response.

form II realization of a single biquad given by, $(b_0 + b_1 z^{-1} + b_2 z^{-2})/(1 + a_1 z^{-1} + a_2 z^{-2})$. The frequency response of an implemented controller (robust $\mathcal{H}_\infty$) is compared with the analytical response in Fig. 13. The slight difference in phase is due to delay in the loop.

V. Characterization of the Device

The range of the X stage was obtained to be 110 μm, and the sensitivity of X LVDT was found to be 6.76 μm/V. As this device has no backlash (as there are no sliding parts) nor any other such design restrictions, the resolution of the device is primarily determined by noise. However, this makes the comparison of the resolution between the open and the closed-loop configurations difficult. Because in the closed-loop designs, the noise is fed back to the actuator, they theoretically cannot achieve better resolutions than the open-loop configurations. However, the open-loop devices are plagued by nonlinear effects such as drift and creep, which make it very difficult to attain these theoretical values in a repeatable and predictable manner. On the other hand, with these nonlinear effects being practically absent, the closed-loop designs provide much better access to accurate positioning. We emphasize here that although theoretically the open-loop resolutions are better (which possibly may be realized with very rigorous experiments and post data processing),

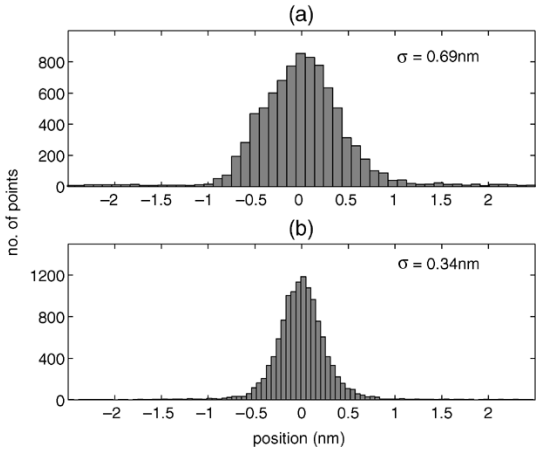

Fig. 14. (a) Open-loop LVDT measurement. (b) LVDT measurement during closed-loop operation.

it is much easier to predict and *realize* accurate positioning in the closed-loop designs.

As the transfer function between x and the noise n is $T(x = Tx_r - Tn)$ it forms a good basis to characterize resolution and compare different designs. This transfer function reveals the tradeoff that exists between the resolution and the bandwidth. This is seen from the fact that higher bandwidth implies larger error signals and therefore worse resolutions. The resolutions can be characterized by associating appropriate metrics to the error signals $e_x = Tn$ if enough statistics describing n is available. This presents us the other problem we have in the characterization of the resolution. Our measurements are limited by the resolution of the LVDT sensors, i.e., the device is capable of motions that are smaller than what LVDT can detect. However, to get a quantitative feel of how small these error signals can be, the following experiment was done. The LVDT signals for both the open- and closed-loop (Glover–McFarlane) designs were measured when the system is at the nominal operating point. The measurement was taken over a small time window as in open loop the mean varies with drift, creep etc. Fig. 14 shows that the variance of the sensor output while in open loop is higher than that in closed loop. This illustrates the improvement in "resolution" due to feedback. As the closed-loop resolution depends on the bandwidth and the shape of the corresponding complementary sensitivity functions better resolutions can be achieved by reducing the bandwidth.

As mentioned earlier, the application of the piezoactuated devices is greatly limited by nonlinear effects such as hysteresis and creep. However these effects are nearly eliminated by the feedback designs described earlier.

VI. Conclusion

This paper describes a procedure for a systematic control design and analysis of large-range nano-positioners. In large-range nano-positioners, along with bandwidth and resolution, robustness assumes great significance. A robust linear controller is needed to tackle the nonlinearities associated with piezoactuation and the changing flexure dynamics without having to design specific nonlinear controllers. The design goals of robustness, bandwidth and resolution can be quantified

in a straightforward manner in the framework of modern robust control. Two approaches are employed to build controllers that provide high robustness while maintaining or improving the stringent bandwidth and resolution requirements. The Glover–McFarlane design is particularly attractive when the need is to robustify an existing controller with specific tracking requirements such as having to track ramp signals with zero steady-state error. It also has the advantage of not having to characterize the uncertainty explicitly. If there is no specific tracking requirement and if an *a priori* characterization of uncertainty is available, then a robust $\mathcal{H}_\infty$ design is found to be attractive for nano-positioning. These design methodologies are experimentally demonstrated on a two-dimensional large-range nano-positioner. The analytic and experimental sensitivity and complementary sensitivity functions along with tracking results demonstrate the merits of the design. The infinity norm of S is chosen to be the measure of robustness in comparing the various design schemes.

ACKNOWLEDGMENT

The authors would like to acknowledge the constant support of Prof. M. Salapaka of Iowa State University and Dr. J. Cleveland of Asylum Research. They would also like to thank T. Day, D. Bocek, Dr. M. Viani, and the rest of Asylum Research for all of their assistance.

REFERENCES

[1] B. C. Crandall, *Nanotechnology: Molecular Speculation on Global Abundance*. Cambridge, MA: MIT Press, 1996.
[2] B. Bhushan, *Handbook of Micro/Nano Tribology*. Boca Raton, FL: CRC, 1995.
[3] M. Yves, *Scanning Probe Microscopes*. Bellingham, WA: SPIE, 1995.
[4] D. R. Meldrum, W. H. Pence, S. E. Moody, D. L. Cunningham, M. Holl, P. J. Wiktor, M. Saini, M. P. Moore, L.-S. Jang, M. Kidd, C. Fisher, and A. Cookson, "Automated, integrated modules for fluid handling, thermal cycling and purification of dna samples for high throughput sequencing and analysis," in *Proc. IEEE/ASME Int. Conf. Advanced Intelligent Mekatronics*, vol. 2, Jul. 2001, pp. 1211–1219.
[5] R. Zhu, D. Xiang, Z. Yang, and J. Chen, "Research on systems for measurements of CCD parameters," *Proc. SPIE-Int. Soc. Opt. Eng.*, vol. 3553, pp. 297–301, Sep. 1998.
[6] D. Krogmann, H. D. Tholl, P. Schreiber, A. Krehl, R. Goring, B. Gotz, and T. Martin, "Image multiplexing system on the base of piezoelectrically driven silicon microlens arrays," in *Proc. 3rd Int. Conf. Micro Opto Electro Mechanical Systems (MOEMS'99)*, Mainz, Germany, Aug.–Sep. 1999, pp. 178–185.
[7] J. Ma and H. A. Marcelo Jr., "High-bandwidth macro/microactuation for hard disk drive," *Proc. SPIE-Int. Soc. Opt. Eng.*, vol. 4194, pp. 94–102, Nov. 2000.
[8] D. L. White and O. R. Wood, "Novel alignment system for imprint lithography," *J. Vac. Sci. Technol. B, Microelectron. Nanometer Structures)*, vol. 18, no. 6, pp. 3552–3556, May–Jun. 2000.
[9] X. Ding and Y. Liu, "Driving technology of micropumps," *J. Electron Devices*, vol. 24, no. 1, pp. 87–92, Mar. 2001.
[10] G. M. Whitesides and H. C. Love, "The art of building small," *Sci. Amer.*, vol. 285, no. 3, pp. 39–47, Sep. 2001.
[11] S. Salapaka, A. Sebastian, J. P. Cleveland, and M. V. Salapaka, "High bandwidth nano-positioner: a robust control approach," *Rev. Sci. Instrum.*, vol. 73, no. 9, pp. 3232–3241, Sep. 2002.
[12] M. Tsai and J. Chen, "Robust tracking control of a piezoactuator using a new approximate hysteresis model," *J. Dyn. Syst., Meas. Control*, vol. 125, pp. 96–102, Mar. 2003.
[13] R. Koops and G. A. Sawatzky, "New scanning device for scanning tunneling microscope applications," *Rev. Sci. Instrum.*, vol. 63, no. 8, pp. 4008–4009, Aug. 1992.
[14] H. Kaizuka, "Application of capacitor insertion method to scanning tunneling microscopes," *Rev. Sci. Instrum.*, vol. 60, no. 10, pp. 3119–3122, 1989.
[15] R. C. Barrett and C. F. Quate, "Optical scan-correction system applied to atomic force microscopy," *Rev. Sci. Instrum.*, vol. 62, pp. 1393–1399, 1991.
[16] D. Croft, G. Shedd, and S. Devasia, "Creep, hysteresis and vibration compensation for piezoactuators: atomic force microscopy application," *J. Dyn. Syst., Meas. Control*, vol. 123, pp. 35–43, 2001.
[17] A. Daniele, S. Salapaka, M. V. Salapaka, and M. Dahleh, "Piezoelectric scanners for atomic force microscopes: design of lateral sensors, identification and control," in *Proc. Amer. Control Conf.*, San Diego, CA, Jun. 1999, pp. 253–257.
[18] G. Schitter, P. Menold, H. F. Knapp, F. Allgower, and A. Stemmer, "High performance feedback for fast scanning atomic force microscopes," *Rev. Sci. Instrum.*, vol. 72, no. 8, pp. 3320–3327, Aug. 2001.
[19] A. Sebastian and S. Salapaka, "$\mathcal{H}_\infty$ loop shaping design for nanopositioning," in *Proc. Amer. Control Conf.*, Denver, CO, Jun. 2003, pp. 3708–3713.
[20] P. O. Kettunen, *Plastic Deformation and Strain Hardening* . Zurich, Switzerland: Trans Tech Publications, 2003.
[21] S. Skogestad and I. Postlethwaite, *Multivariable Feedback Control, Analysis and Design*. New York: Wiley, 1997.
[22] K. Glover and D. McFarlane, "Robust stabilization of normalized coprime factor plant descriptions with $\mathcal{H}_\infty$-bounded uncertainty," *IEEE Trans. Autom. Control*, vol. 34, no. 8, pp. 821–830, Aug. 1989.
[23] D. McFarlane and K. Glover, "A loop shaping design procedure using $\mathcal{H}_\infty$ synthesis," *IEEE Trans. Autom. Control*, vol. 37, no. 6, pp. 759–769, Jun. 1992.
[24] J. Sefton and K. Glover, "Pole/zero cancellations in the general $\mathcal{H}_\infty$ problem with reference to a two block design," *Syst. Control Lett.*, vol. 14, no. 4, 1990.
[25] S. K. Mitra, *Digital Signal Processing: A Computer Based Approach*, 2nd ed. New York: McGraw-Hill, 1999.

Abu Sebastian (M'01) was born in Kerala, India, in 1977. He received the B.E. (Hons.) degree in electrical and electronics engineering from Birla Institute of Technology and Science, Pilani, India, in 1998 and the M.S. and Ph.D. degrees in electrical engineering from Iowa State University, Ames, in 1999 and 2004, respectively.

He is currently with the IBM Zürich Research Laboratory, Rüschlikon, Switzerland. His research is primarily focused on the application of control theory to nano-scale devices. He has worked on the analysis of atomic force microscope dynamics and the development of novel modes of operation based on a systems perspective. Other research interests include nanopositioning and probe-based data storage.

Srinivasa M. Salapaka (M'93) was born in Andhra Pradesh, India, in 1973. He received the B.Tech. degree in mechanical engineering from the Indian Institute of Technology, Chennai, in 1995 and the M.S. and Ph.D. degrees in mechanical engineering from the University of California at Santa Barbara in 1997 and 2002, respectively.

From 2002 to 2004, he was a Postdoctoral Associate in the Laboratory for Information and Decision Systems, Massachusetts Institute of Technology, Cambridge. Since 2004, he has been a Faculty Member in Mechanical Engineering, University of Illinois, Urbana-Champaign. His areas of current research interest include controls for nanotechnology, combinatorial resource allocation, and numerical analysis of integral equations.

Dr. Salapaka received the National Science Foundation CAREER Award in 2005.